Available online at www.sciencedirect.com
ScienceDirect
Acta Materialia 56 (2008) 479–488
Acta MATERIALIA
www.elsevier.com/locate/actamat

Piezoelectric bending response and switching behavior of ferroelectric/paraelectric bilayers

Yue Zheng [a,b], Biao Wang [b,c], C.H. Woo [a,*]

[a] Department of Electronic and Information Engineering, The Hong Kong Polytechnic University, Hong Kong, China
[b] Electro-Optics Technology Center, Harbin Institute of Technology, Harbin 150001, China
[c] State Key Laboratory of Optoelectronic Materials and Technologies, Institute of Optoelectronic and Functional Composite Materials and School of Physics and Engineering, Sun Yat-sen University, Guangzhou, China

Received 2 August 2007; received in revised form 1 October 2007; accepted 3 October 2007
Available online 3 December 2007

Abstract

We consider the dynamic piezoelectric bending response and switching behavior of ferroelectric/paraelectric bilayers due to an applied electric field. A thermodynamic model is developed, in which the stresses due to the lattice mismatch and ferroelectric phase transformation are inhomogeneous. The polarization, radius of curvature, and relative vertical displacement due to the bending are calculated and analyzed as a function of the ratio of the thicknesses of the two layers. The bending response is found to be very large, and is highly adjustable by varying the relative thicknesses of the two layers. Our results show ferroelectric/paraelectric bilayers may have very good potential for applications as transducers, sensors and actuators.

Keywords: Ferroelectric; Paraelectric; Bilayer; External electric field

1. Introduction

Ferroelectric or piezoelectric materials are used extensively as transducers, sensors and actuators for signals of various kinds of external fields, including electric, magnetic, temperature, pressure, vibration or noise etc [1–12]. These materials are popular for smart structure design because they are light, compact, relatively inexpensive, and exhibit moderately linear field-strain relations at low drive levels, and are particularly suited to aerospace, aeronautic, industrial and biomedical applications. Furthermore, an inherently non-linear and hysteric constitutive behavior gives rise to many interesting properties [1].

Much effort has been devoted to increase the displacement sensitivities of actuators and sensors by making use of multilayer and composite actuator/sensor structures such as bimorphs [13], moonies [14], and cymbals [15,16]. To enhance the small displacements, various types of strain-amplifying architectures have also been developed. For example, a flex-tensional actuator composed of a PZN-PZT layer and a PZN-PZT/Ag layer was developed by Yoon et al. [17], the displacement of which was remarkably enhanced with inter-digital electrodes. To supplement the design effort, analysis of the stress distribution and curvature in multilayer and composite layers were performed [18,19] using elasticity theory.

In addition, physical properties of ferroelectric thin films grown on substrate depend very much on surface and boundary effects. Pertsev et al. [20] reported on the effect of mechanical boundary conditions on the polarization, dielectric constants and phase diagram of ferroelectric film grown on a substrate. Bhattacharya and James [21] developed a theory of deformation to study the behavior of the martensitic films grown on a substrate with finite thickness. Our previous works [22,23] have also shown that the epitaxial stress significantly affects the transformation in

* Corresponding author. Tel.: +852 2766 6646.
E-mail addresses: yuezheng@hit.edu.cn (Y. Zheng), stdwangb@zsu.edu.cn (B. Wang), chung.woo@polyu.edu.hk (C.H. Woo).

1359-6454/$30.00
doi:10.1016/j.actamat.2007.10.011

general, changing the Curie temperature, the Curie–Weiss relation and the magnitude of the polarization, or even change a first-order bulk ferroelectric to undergo second-order phase transition in the thin film form.

In this work, we consider the effects of film/substrate thicknesses on the polarization distribution, piezoelectric bending response and switching behavior of a ferroelectric/paraelectric (FE/PE) bilayer system. We are particularly interested in the relative vertical displacement of the bending bilayer as a function of the geometry and the actuating field.

2. Formulation

2.1. The free energy

We consider the FE/PE bilayer system shown in Fig. 1a, where h and H are the thicknesses of the respective layers, and L is the common lateral dimension. The coordinate system is defined such that the interface is at $z = 0$, and the free surfaces at $z = h$ and $z = -H$, respectively.

As in our previous formulation [22–24], the ferroelectric is considered as an assembly of polar molecules (crystallographic unit cells) occupying a volume V in space. Following the classical description of electrical susceptibility of a collection of polar molecules [25] (crystallographic unit cells) the total polarization $\mathbf{P}^{\mathrm{T}}$ at any spatial location may be considered as composed of a non-linear structural component $\mathbf{P}$ and a linear induced component $\mathbf{P}^{\mathrm{E}}$ that is proportional to the electric field $\mathbf{E}$ with a constant susceptibility χ_{d}. To properly reflect the non-linear behavior of the free energy in the neighborhood of system instability it is necessary to separate the two contributions. The electric displacement is then given by

$$\mathbf{D} = \varepsilon_0\mathbf{E} + \mathbf{P}^{\mathrm{T}} = \varepsilon_0\mathbf{E} + \mathbf{P}^{\mathrm{E}} + \mathbf{P} = \varepsilon_0\mathbf{E} + \chi_{\mathrm{d}}\mathbf{E} + \mathbf{P} = \varepsilon_{\mathrm{d}}\mathbf{E} + \mathbf{P}$$

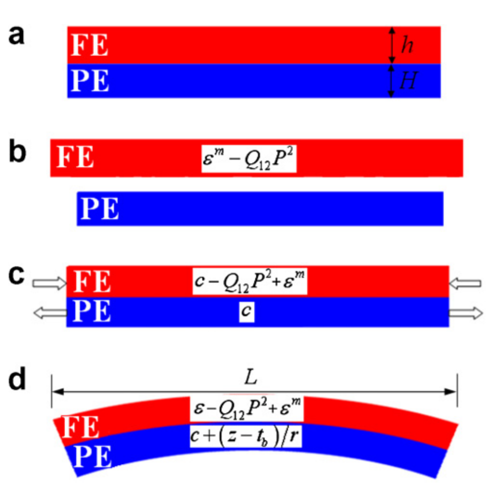

Fig. 1. Schematic diagrams showing: (a) the FE/PE bilayer system, (b) unconstrained strains due to the misfit strain and self-phase-transformation strains, (c) constrained strains to main displacement compatibility, and (d) bending induced by asymmetric stresses.

where ε_0 are dielectric constants of the vacuum. ε_{d} is the dielectric constant of the current phase of the background material [24–30].

To simplify discussions, we consider the one-dimensional problem in which the polarization is directed along the plate thickness such that $P_1 = P_2 = 0$ and $P_3 = P(z)$, i.e., independent of x and y. The total free energy per unit area of the bilayer can then be written as

$$F = F_0 + F_{\mathrm{P}} + F_{\mathrm{Ela}} + F_{\mathrm{Ele}} = F_0 + \int_{-H}^{h} (f_{\mathrm{P}}(z) + f_{\mathrm{Ela}}(z) + f_{\mathrm{Ele}}(z))\mathrm{d}z \quad (1)$$

where F_{P} is the self-energy of the reference state which, in the present case, is the field-free (electrical and mechanical) infinite crystal. F_{Ela} and F_{Ele} are contributions due to actions on the reference state caused by mechanical stresses and electric fields in the finite crystal, respectively. f_{P}, f_{Ela} and f_{Ele} are the corresponding energy densities. F_0 is the free energy component that is independent of the polarization. To concentrate on the mechanical behavior of the system in this study, we consider cases where surface effects such as depolarization and surface relaxation [23] are negligible. At the same time, we will only discuss mechanical behavior of FE/PE system far away from the phase transition temperature T_{c}, which is mainly determined by the misfit between film and substrate [23]. For simplicity, the effect of the induced polarization on the mechanical behavior is neglected in this work [28].

We first consider the elastic energy contribution FEla due to the lattice misfit of the materials in the bilayer. Let as be the lattice constant of PE layer and af the equivalent cubic cell constant of the free-standing FE layer. Assuming a coherent interface, the biaxial in-plane misfit strain in the film εm can be written as [22] $\varepsilon^m_{11} = \varepsilon^m_{22} = \varepsilon_m = (a_{\mathrm{s}} - a_{\mathrm{f}})/a_{\mathrm{f}}$.

In addition to the misfit, we also have a transformation strain associated with the polarization generated by the lattice instability. In the following, we only consider the case of a FE layer grown on a compressive PE layer (i.e. as < af). We assume that the polarization P is along the z direction and the transformation strains determined by the polarization can be expressed as $\varepsilon^{\mathrm{T}}_{11} = \varepsilon^{\mathrm{T}}_{22} = \varepsilon^{\mathrm{T}} = Q_{12}P^2$, where Q12 is the electrostrictive coefficient. We consider both the FE and PE layers are cubic elastic media with moduli C_{11}, C_{12}; $\bar{C}_{11}, \bar{C}_{22}$, respectively. The effective elastic constants are given by $G = C_{11} + C_{12} - 2C^2_{12}/C_{11}$ and $\bar{G} = \bar{C}_{11} + \bar{C}_{12} - 2\bar{C}^2_{12}/\bar{C}_{11}$.

Stresses in the bilayer are thus created by the combined effects of the misfit and transformation strains, which can be calculated following the treatment of Hsueh and Evans [31–34]. Thus, starting with uncoupled FE and PE layers that experience unconstrained and incompatible in-plane strains $\varepsilon_{11} = \varepsilon_{22} = \varepsilon^m - Q_{12}P^2$ and $\bar{\varepsilon}_{11} = \bar{\varepsilon}_{22}$ [22,34,35], respectively (Fig. 1b), uniform stresses, corresponding to the uniform strain c, are then imposed on each of the two layers to maintain displacement compatibility and equilibrium (Fig. 1c). In this procedure, the resultant force (per unit length) N created by the misfit and the electrostrictive stresses in the FE layer $\sigma_{\text{appl}} = G(\varepsilon^m - Q_{12}P^2)$, due to the constraint of the PE layer, is given by

$$N = \int_0^h \sigma_{\text{appl}}\,dz = \int_0^h G(\varepsilon^m - Q_{12}P^2)dz$$

At equilibrium, the balancing force $-N$ is provided by a uniform elastic strain $c = -N/(hG + H\bar{G})$ in the PE layer [36]. The total elastic strain is then $c - Q_{12}P^2 + \varepsilon^m$ in the FE layer, and c in the PE layer (Fig. 1c). Finally, relaxing the constraint of strain uniformity, bending of the system occurs because of the development of asymmetric stresses as shown in Fig. 1d. In the final configuration, the strain depends on z and can be written as

$$\begin{aligned} &\varepsilon_s = \varepsilon = c + \frac{z - t_b}{r} \quad \text{for } -H \leqslant z \leqslant 0 \\ &\varepsilon_f = \varepsilon - Q_{12}P^2 + \varepsilon^m = c + \frac{z - t_b}{r} - Q_{12}P^2 + \varepsilon^m \quad \text{for } 0 \geqslant z \geqslant h \end{aligned} \tag{2}$$

where $z = t_b$ is the location of the bending axis, which is different from the conventional neutral axial. r is the radius of curvature of the system. According to Eq. (2) the strain is proportional to the distance from the bending axis and inversely proportional to the radius of curvature.

Taking into account both the misfit and transformation strains, the stresses σ_s and σ_f in the substrate and film, respectively, are given by

$$\begin{aligned} &\sigma_s = \bar{G}\varepsilon \quad \text{for } -H \leqslant z \leqslant 0 \\ &\sigma_f = G(\varepsilon - Q_{12}P^2 + \varepsilon^m) \quad \text{for } 0 \geqslant z \geqslant h \end{aligned} \tag{3}$$

The strain distributions in the FE/PE bilayer system are contingent upon solutions of the three parameters, c, t_b and r, which can be determined sequentially from the following three equilibrium conditions.

Firstly, zero resultant force in Fig. 1c gives

$$\int_{-H}^0 \bar{G}c\,dz + \int_0^h G(c + \varepsilon^m - Q_{12}P^2)dz = 0 \tag{4}$$

The uniform strain component c from Eq. (4) is then given by

$$c = -\frac{Gh(\varepsilon^m - \frac{Q_{12}}{h}\int_0^h P^2\,dz)}{\bar{G}H + Gh} \tag{5}$$

Secondly, the force equilibrium in Fig. 1d requires

$$\int_{-H}^0 \bar{G}\frac{z - t_b}{r}\,dz + \int_0^h G\frac{z - t_b}{r}\,dz = 0 \tag{6}$$

from which the position of the bending axis t_b can be determined

$$t_b = \frac{Gh^2 - \bar{G}H^2}{2(Gh + \bar{G}H)} \tag{7}$$

Thirdly, the torque equilibrium in Fig. 1d requires

$$\int_{-H}^0 \sigma_s z\,dz + \int_0^h \sigma_f z\,dz = \int_{-H}^0 \bar{G}\varepsilon(z)z\,dz + \int_0^h G[\varepsilon(z) + \varepsilon^m - Q_{12}P^2]z\,dz = 0 \tag{8}$$

from which the radius of the curvature r can be determined from Eqs. (4)–(8) to give

$$r = \frac{\bar{G}H^2(2H + 3t_b) + Gh^2(2h - 3t_b)}{3(\bar{G}cH^2 - Gch^2 - G\varepsilon^m h^2 + 2GQ_{12}\int_0^h P^2 z\,dz)} \tag{9}$$

Finally, the total elastic energy F_{Ela} of the bilayer is given by

$$\begin{aligned} F_{\text{Ela}} &= \frac{1}{2}\int_{-H}^h (\sigma_1(z)\varepsilon_1(z) + \sigma_2(z)\varepsilon_2(z))dz \\ &= \int_{-H}^0 \bar{G}\varepsilon(z)\varepsilon(z)dz + \int_0^h G\big[-2[\varepsilon(z) + \varepsilon^m]Q_{12}P^2(z) \\ &\quad + Q_{12}^2P^4(z) + (\varepsilon^m)^2 + \varepsilon^2(z) + 2\varepsilon(z)\varepsilon^m\big]dz \end{aligned} \tag{10}$$

The free energy of our reference state F_P in the first term of Eq. (1) is now considered. F_P can be written as the sum of the non-linear Landau free energy functional for a field-free and uniform infinite crystal and the Ginzburg contribution to account for the presence of non-uniformity in P

$$F_P = \int_0^h \frac{1}{2}A(T - T_{c0})P^2 + \frac{1}{4}BP^4 + \frac{1}{6}CP^6 + \frac{1}{2}D\left(\frac{dP}{dz}\right)^2 dz \tag{11}$$

where A, B and C are the expansion coefficients of the Landau free energy, and D can be approximated as $\xi^2 \cdot |A(T - T_{c0})|$, ξ is a characteristic length along which the polarization varies.

The last term in Eq. (1) has contributions from the depolarization and external electric fields E_d and E_{ext}, respectively. As a result of possible charge compensation, such as that due to oxygen vacancies in perovskite ferroelectrics, we may assume for simplicity that E_d is negligible. The contribution F_{Ele} can then be written simply as

$$F_{\text{Ele}} = \int_0^h [-E_{\text{ext}}P(z)]dz \tag{12}$$

2.2. Euler–Lagrange equation and numerical solution

The variation of the total free energy with respect to P [20,23–37] yields the Euler–Lagrange equation for the dynamics of the system, which is often called the time-dependent Ginzberg–Landau equation (TDGL), from which the evolution of the polarization in ferroelectric layer can be calculated

$$\frac{\partial P(z,h,H,t)}{\partial t} = -M\frac{\delta F}{\delta P} = -M\left[A^*(z,h,H,t)P + B^*(z,h,H,t)P^3 + CP^5 - D\frac{d^2P}{dz^2} - E_{\text{ext}}\right], \tag{13}$$

where M is the kinetic coefficient related to the domain wall mobility, and the renormalized coefficients are

$$A^*(z,h,H,t) = A(T - T_{c0}) - 4GQ_{12}\left[c(h,H,t) + \frac{z - t_b(h,H)}{r(h,H,t)} + \varepsilon^m\right],$$

$$B^* = B + 4GQ_{12}^2.$$

From Eqs. (3)–(10), the evolution of the polarization, the uniform strain component, the position of the bending axis, and the radius of the curvature can be calculated as functions of FE layer thickness h, PE layer thickness H and evolution time t:

$$c(h,H,t) = -\frac{Gh}{\bar{G}H + Gh}\left(\varepsilon^m - Q_{12}\frac{1}{h}\int_0^h P(t)\mathrm{d}z\right),$$

$$t_b(h,H) = \frac{Gh^2 - \bar{G}H^2}{2(Gh + \bar{G}H)},$$

$$r(h,H,t) = \frac{\bar{G}H^2(2H + 3t_b) + Gh^2(2h - 3t_b)}{3\left(\bar{G}cH^2 - Gch^2 - G\varepsilon^m h^2 + 2GQ_{12}\int_0^h P^2(t)z\,\mathrm{d}z\right)} \tag{14}$$

Eq. (13) can be solved numerically to yield the steady-state polarization distribution and the corresponding gradient, and the mechanical force balance from Eqs. (4), (6), and (8). The polarization profile $P(z)$ along the z direction and the average polarization $\langle P\rangle = \int_0^h P\,\mathrm{d}z/h$ can be obtained from the solution of Eq. (13). From Eqs. (5), (7), and (9), respectively, the uniform strain component c, the position of the bending axis t_b, and the radius of the curvature r can also be determined.

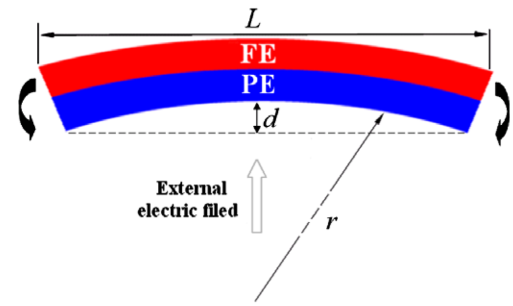

Fig. 2. Schematic diagram showing bending of FE/PE bilayer due to a applied external electric fields. Inhomogeneous stress distribution in FE/PE bilayer result in a radius of curvature r and a dome-shaped bending with displacement d.

2.3. The stationary and relative displacements

Solving Eqs. (13) and (14), stationary values of the polarization P_∞, uniform strain component c_∞, and radius

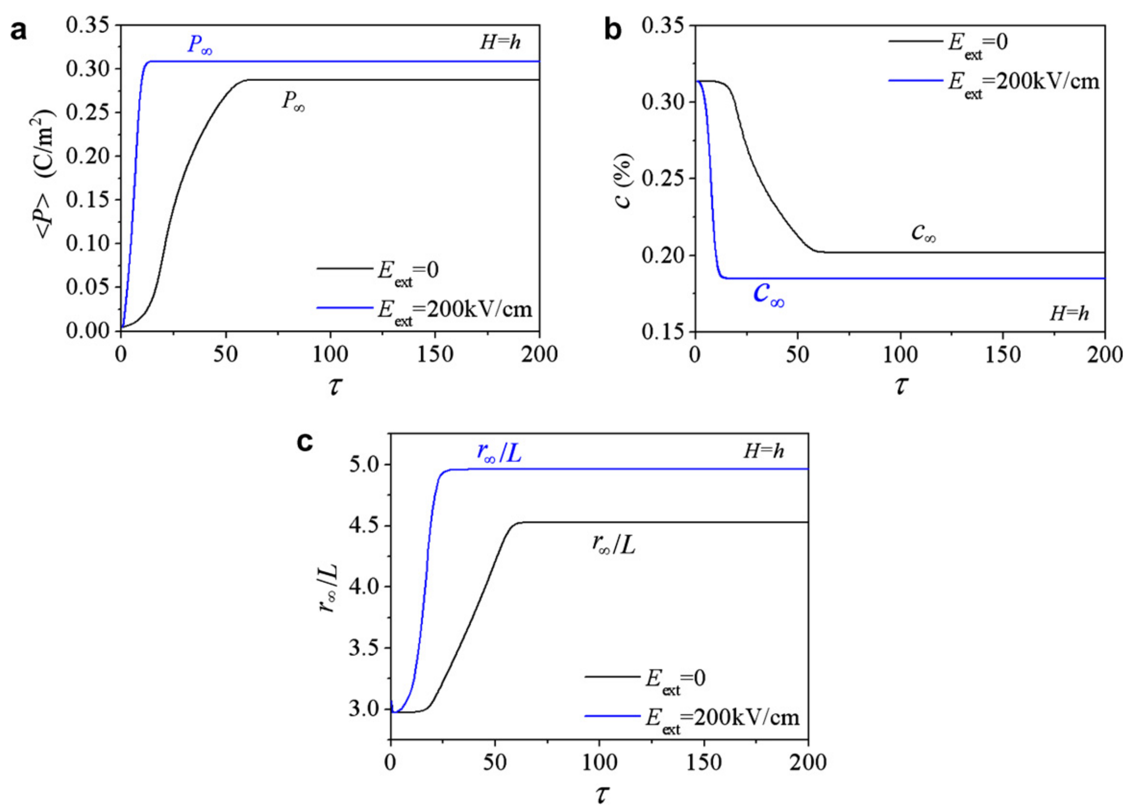

Fig. 3. (a) The polarization, (b) the uniform strain component, and (c) the radius of the curvature from the solution of the TDGL equation (18). The general time is $\tau \times 10^{-9}$. The calculation is done for $H = h = 0.1$ mm. The black line is for a static applied electric field of $E_{ext} = 0$ and the blue line for $E_{ext} = 200\ \mathrm{kV\,cm^{-1}}$. Evolution from the unpolarized unstable state to the polarized stationary state can be clearly seen. (For interpretation of the references to color in this figure legend, the reader is referred to the web version of this article.)

of the curvature r_∞ can be obtained at $\tau > \tau_s$. In this solution, we have used the generalized evolution time $\tau = Mt = N\Delta\tau = NM\Delta t$ [23,24,26], where Δt is the real time step and $\Delta\tau = M\Delta t$ is the effective time step. N is the total number of the time steps. τ_s is the time after which P, c and r becomes stationary.

According to Fig. 2, the stationary bending displacement due to E_{ext} is given by

$$d_\infty(E_{ext}) = r_\infty - \sqrt{r_\infty^2 - \left[\sin\left(\frac{L}{2}\right)\right]^2} \tag{15}$$

We define the relative displacement in terms of the static ones by

$$\Delta D(E_{ext}) = \frac{d_\infty(E_{ext}) - d_\infty(E_{ext} = 0)}{\bar{H}(h, H)} \tag{16}$$

where $\bar{H} = h + H$ is the total thickness of the bilayer. The relative displacement measures the piezoelectric bending response due to the applied electric field only.

2.4. Piezoelectric response of the bilayer under a cyclic electric field

Under a cyclic sinusoidal external field E_{ext} along the z direction as in [26,37,38,39]:

$$E_{ext} = E_0 \sin\left(\frac{2\pi t}{T'}\right) = E_0 \sin(2\pi t f') \tag{17}$$

where E_0, T' and f' are the amplitude, period and frequency, respectively. The time evolution of the system is governed by the TDGL equation:

$$\frac{\partial P(z, h, H, E_0, t)}{\partial t} = -M \frac{\delta F}{\delta P(z, h, H, E_0, t)}, \tag{18}$$

The mechanical responses of the system, the evolution of the polarization $P(z, h, H, t)$, the uniform strain component $c(h, H, t)$, the position of the bending axis $t_b(h, H, t)$, and the radius of the curvature $r(h, H, t)$ can be obtained numerically by solving Eqs. (17) and (18) via Eq. (13).

The dynamic and relative displacements of our system can then be calculated according to Eqs. (15) and (16):

$$d[E_{ext}(E_0, t)] = r(E_0, t) - \sqrt{r(E_0, t)^2 - \left[\sin\left(\frac{L(E_0, t)}{2}\right)\right]^2} \tag{19}$$

and

$$\Delta D[E_{ext}(E_0, t)] = \frac{\mathrm{d}[E_{ext}(E_0, t)] - \mathrm{d}(E_{ext} = 0)}{\bar{H}(h, H)} \tag{20}$$

3. Results and discussions

The following results and discussions refer to the specific example of the $BaTiO_3/SrTiO_3$ bilayer system. The lattice constants of $BaTiO_3$ layer and $SrTiO_3$ layer are

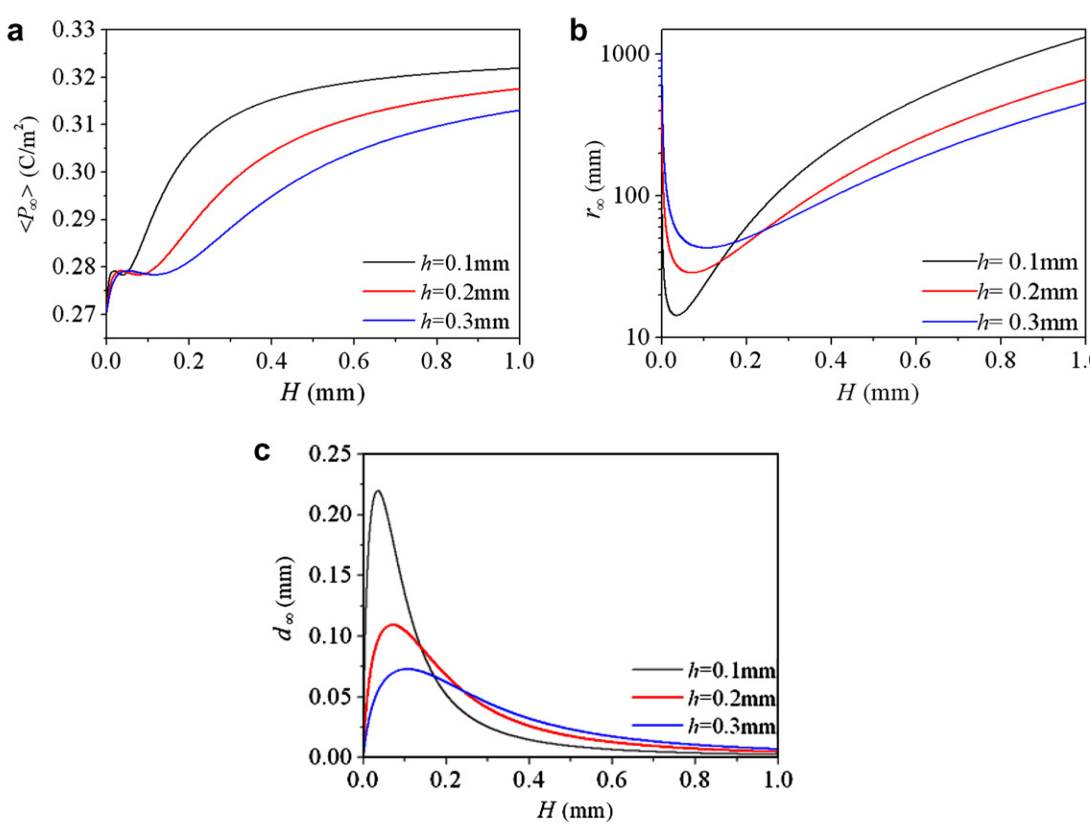

Fig. 4. (a) The average polarization, (b) normalized static radius of curvature, and (c) normalized static displacement, as functions of the thickness of the PE substrate H for various FE film thickness h.

$a_f = 0.401$ and $a_s = 0.3905$, respectively. The material constants for the Landau free energy, the electrostrictive coefficients and the elastic properties are from Refs. [20,40,41]. We firstly consider that the thickness h_1 of the FE layer is 0.1 mm, and the lateral dimension L is $50h_1$.The generalized time step used is $\Delta\tau = 0.1 \times 10^{-9}$. In Fig. 3a, we show the spontaneous growth from zero to a final stationary value of the average polarization in the FE layer under static external electric fields $E_{ext} = 0$ and $E_{ext} = 20\ \text{kV cm}^{-1}$. Fig. 3b and c shows the respective stationary values of the corresponding uniform strain component and radius of the curvature. The generalized time τ in these figures is in unit of 0.2×10^{-6}.

3.1. Stationary polarization, curvature and bending displacement with external electric field

In Fig. 4a we plot the stationary average polarization $\langle P_\infty \rangle$ calculated using the foregoing procedure as a function of H, for various thickness of the FE film h. This result shows that the average polarization is a strong function of h for all values of H except the very small ones. $\langle P_\infty \rangle$ can be seen to vary between two limits of H: one in which H is large and the FE layer is totally constrained by a thick PE substrate, and another in which H is small and the FE layer is free standing and unconstrained. The small peak of $\langle P_\infty \rangle$ at $H \approx 0.3h$ is the result of the bending of the bilayer. Fig. 4b and c plots the corresponding radius of curvature and static displacements, respectively, both of which show corresponding minima and maxima at $H \approx 0.3h$. It is interesting to note the very large displacements that can be obtained in the region $H \leqslant h$, where effective strains as large as 100% can be achieved.

3.2. Stationary polarization curvature and bending displacement as function of external electric field

Fig. 5a shows the stationary average polarization $\langle P_\infty \rangle$ as function of the external electric field, for various values of the PE substrate thickness. $\langle P_\infty \rangle$ can be seen to increase with increasing external electric field and increasing substrate thickness. Based on results in Fig. 5a, we also calculate the stationary curvature r_∞ and displacement d_∞. Fig. 5b shows that the stationary curvature increases, while Fig. 5c shows that the stationary displacement decreases, with increasing external electric field. From Eq. (16), we can also calculate the relative displacement as function of external electric field as shown in Fig. 5d. These results confirm the large piezoelectric bending response under applied electric field. In the case of $H = 0.05h$, the relative displacement $|\Delta D|$ can be as high as 18% for an applied electric field $E_{ext} = 500\ \text{kV cm}^{-1}$. For a substrate thickness of $H = 0.5h$, $|\Delta D|$ may increase to 27%. Lower values of $|\Delta D|$, however, are obtained as the ratio H/h further increases.

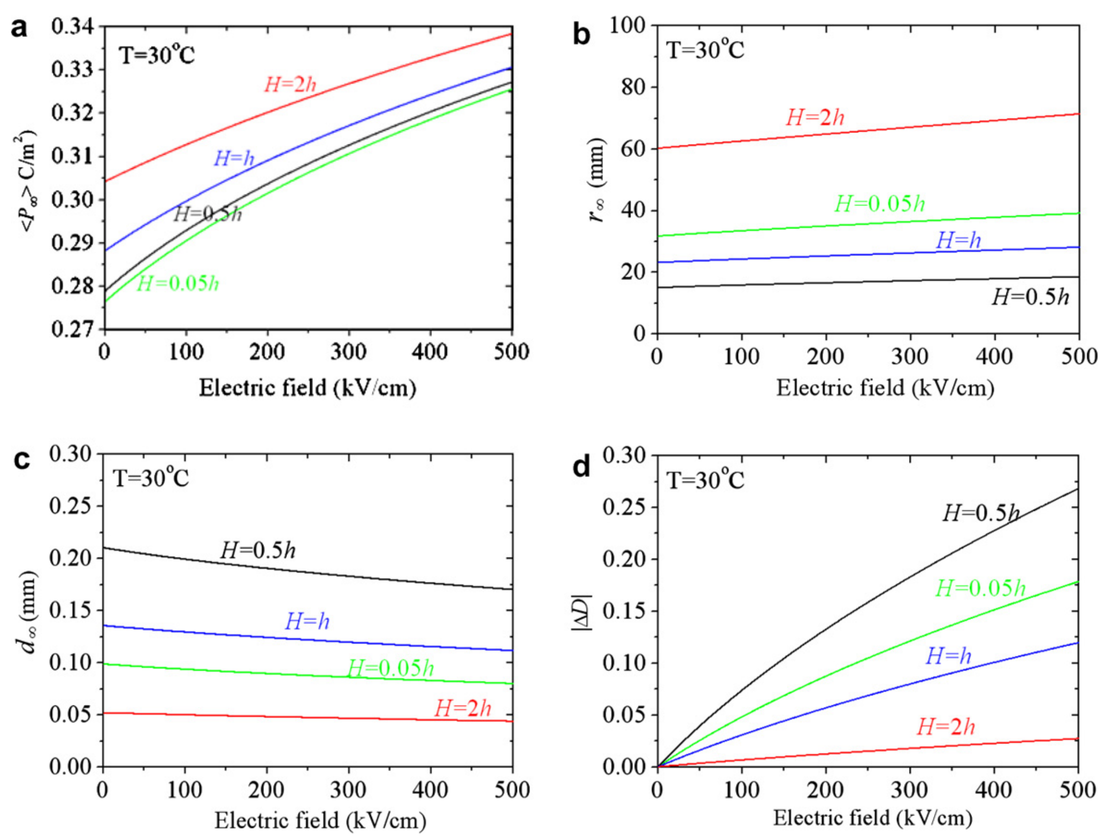

Fig. 5. (a) The average polarization, (b) normalized radius of curvature, (c) normalized static displacement, and (d) the relative displacement, as functions of the applied external electric filed for various substrate thicknesses.

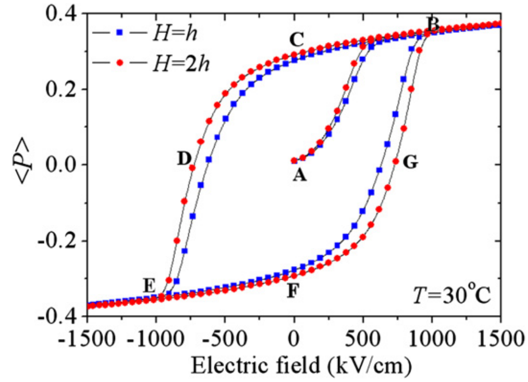

Fig. 6. Hysteresis loops in BTO/STO for $H = h$ (squares), and $H = 2h$ (circles).

3.3. Hysteresis loop

We compare the cases where $H = h = 0.1$ mm and $H = 2h = 0.2$ mm. The average polarization $\langle P \rangle$ is calculated as a function of a sinusoidal applied electric field by solving Eq. (18). In Eq. (17), the amplitude of the external field used is $E_0 = 1500\ \mathrm{kV\,cm^{-1}}$. To alleviate the effect of the frequency of the external electric field on the switching behavior of bilayer system, we use the generalized time step $\Delta\tau = 1 \times 10^{-9}$. Number of time step N in a period is 200.

Fig. 6 shows the corresponding hysteresis loops of $BaTiO_3/SrTiO_3$ bilayer. The remnant polarization P_r and coercive field E_c all see enhancement as H increases.

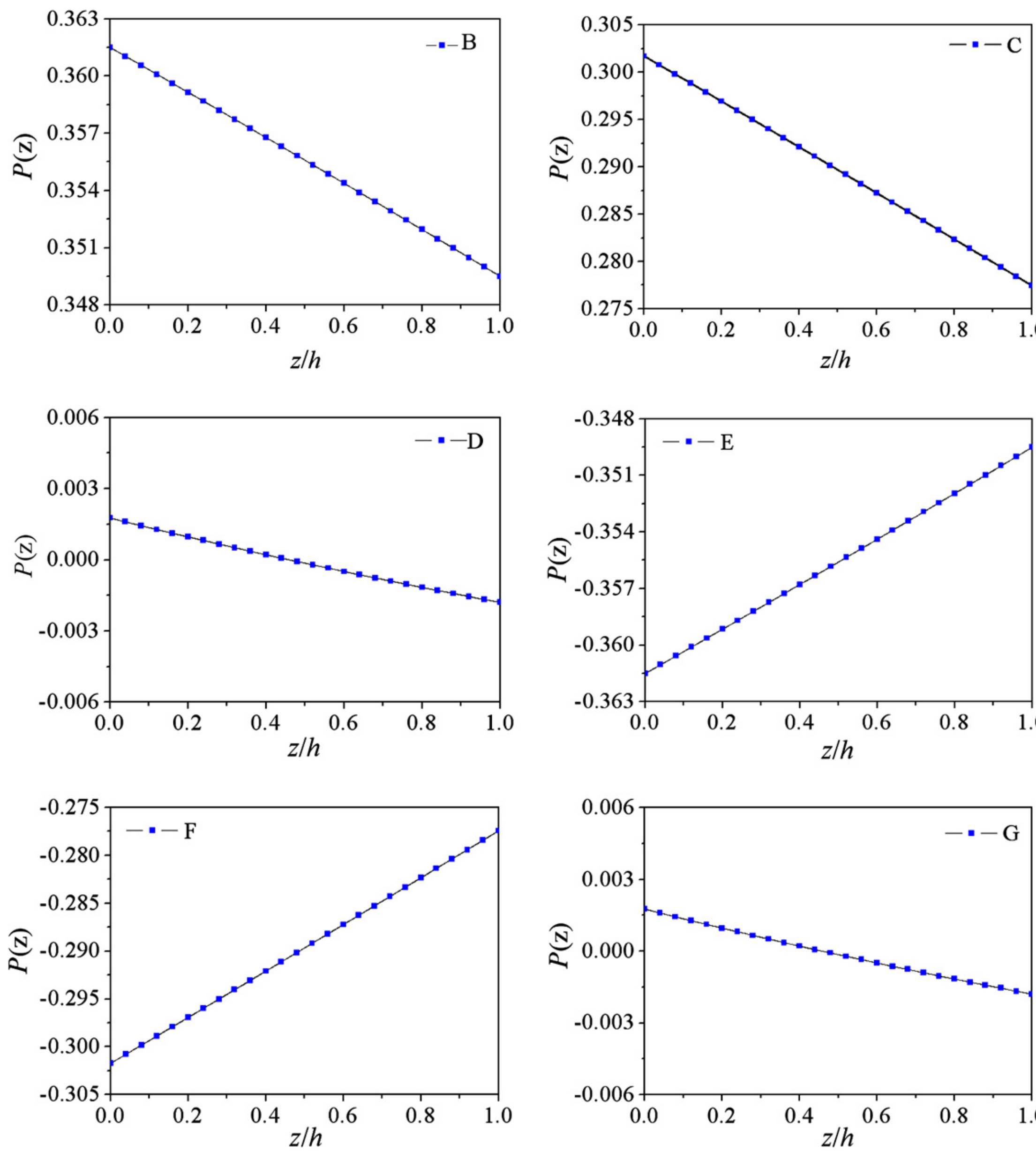

Fig. 7. The polarization distribution at points B, C, D, E, F and G in hysteresis loop of Fig. 6 at the case of $H = h$.

To understand the deformation behavior of the bilayer, we also give the polarization pattern at points B, C, D, E, F and G for $H = h$, as shown in Fig. 7. Here it is obvious that external electric field influences the magnitude and distribution of the polarization, and hence the total strains in FE/PE layer. At the same time, the external electric field also induces the bending deformation of the bilayer, which we will be discussed in the next section.

3.4. Dynamic loading

The dynamic curvature and displacement due to the sinusoidal external electric field of Eq. (17) are calculated and shown in Fig. 8 for a substrate thickness $H = h$. The radius of curvature r is shown in Fig. 8a. The dynamic displacement d can be obtained by solving Eq. (19) (Fig. 8b). It can be seen that the displacement can reach about 200% of FE film thickness at external electric fields $E_{ext} = -730$ (D) and 730 (G) (kV cm^{-1}). When external electric field is large, such as $E_{ext} = -1100$ (E) or 1100 (B) (kV cm^{-1}), the displacement reduces to only about 0.7h. From Fig. 8a and b, the relative dynamic displacement $|\Delta D|$ can also be obtained by solving Eq. (20). The results are plotted in Fig. 8c. It can be seen that $|\Delta D|$ can be as high as 58% for $E_{ext} = -1100$ (E) or 1100 (B) and $H = h$.

To examine the effect of the substrate thickness on the piezoelectric bending response, we also calculate the dynamic curvature, displacement d and relative displacement $|\Delta D|$ of a $BaTiO_3/SrTiO_3$ bilayer for $H = 2h$ and plot the results in Fig. 9. It can be seen that the piezoelectric and bending responses are weakened due to the increase of the substrate thickness. Thus, the relative displacement $|\Delta D|$ in Fig. 9c is only 1/3 of that of Fig. 8c where $H = h$.

Results of Figs 8 and 9 again demonstrate that the FE/PE bilayer system has a large piezoelectric bending response. At the same time, our results also indicate the piezoelectric and bending response can be adjusted via the thicknesses of the PE substrate and the FE film.

4. Summary

In summary, an elastic and thermodynamic model is constructed for investigating the piezoelectric and bending response of a FE/PE bilayer system. Taking into account effects of the misfit and transformation strains, we obtain static and dynamic polarization, curvature and displacement as a function of the film/substrate thicknesses of the bilayer. Our results show that both the static and dynamic piezoelectric and bending responses due to the inhomogeneous stress in the bilayer can produce large vertical dis-

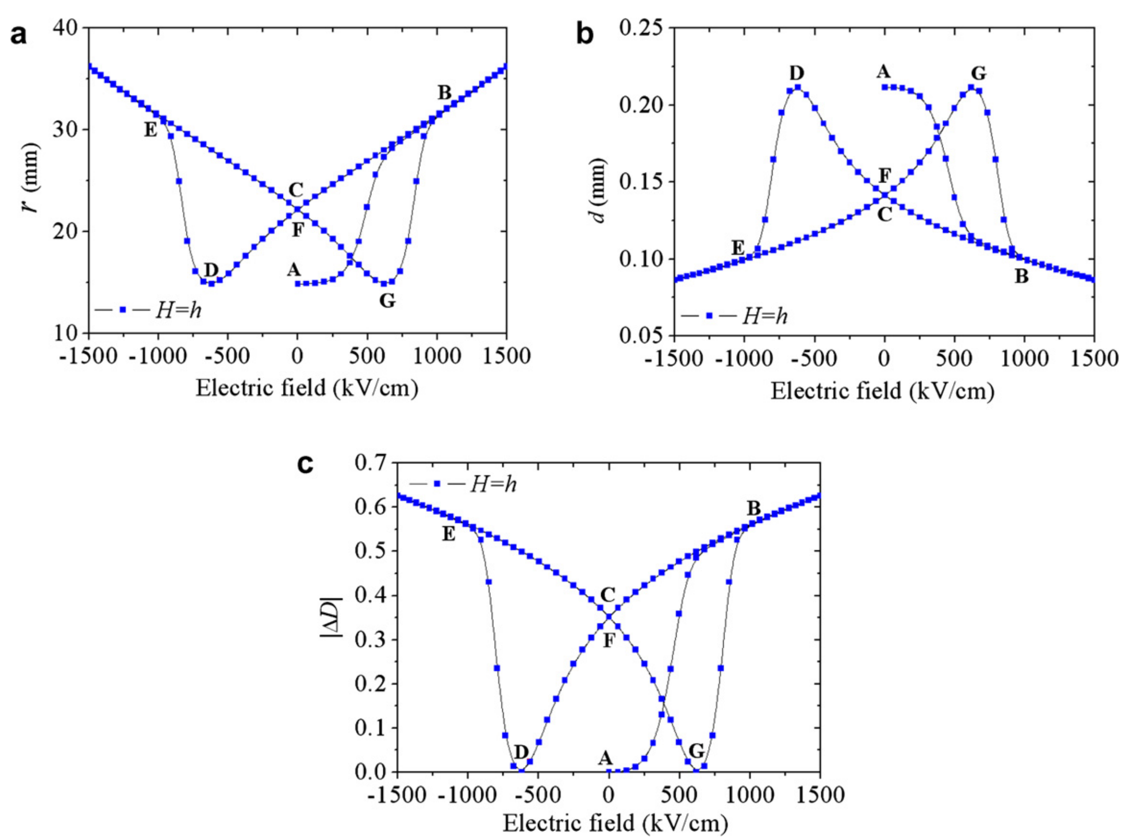

Fig. 8. Dynamics of: (a) the radius of curvature, (b) displacement of bonding bilayer, and (c) relative displacement of bonding bilayer subjected to a sinusoidal applied electric field ($H = h$).

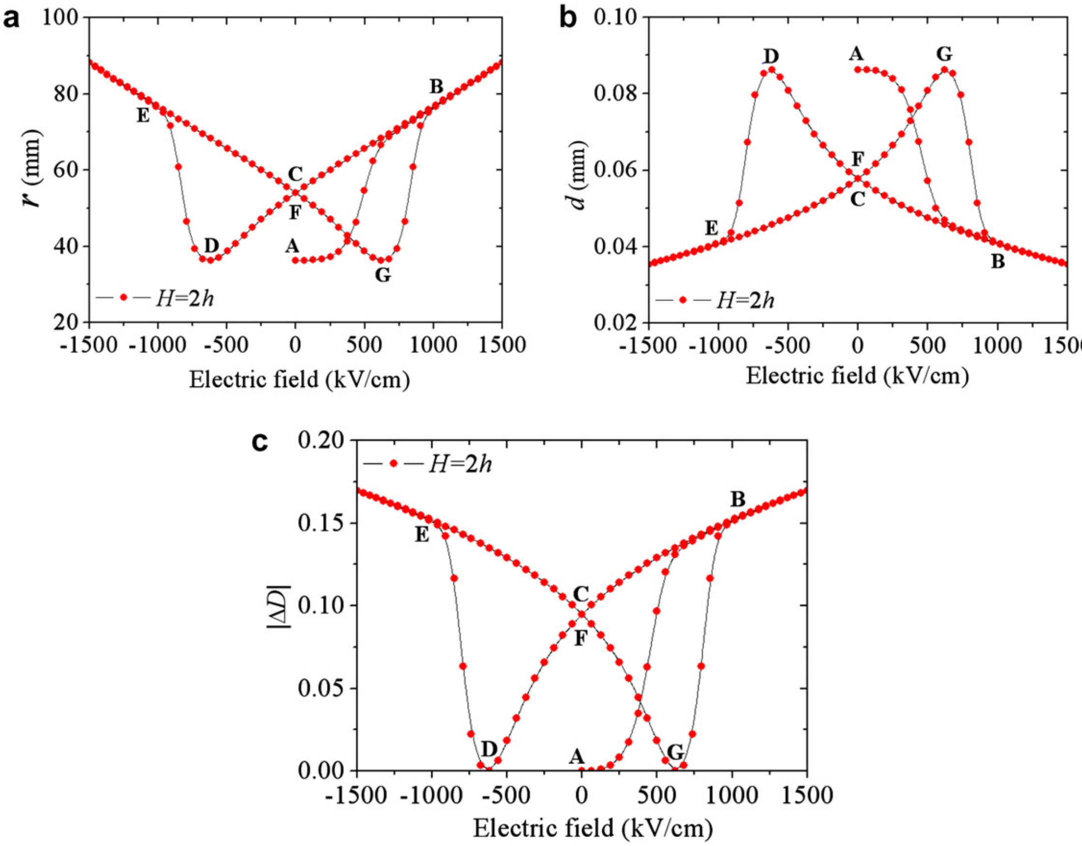

Fig. 9. Dynamics of: (a) the radius of curvature, (b) displacement of bonding bilayer, and (c) relative displacement of bonding bilayer subjected to a sinusoidal applied electric field ($H = 2h$).

placements. At the same time, this displacement, together with the associated polarization, radius of curvature, and vertical displacement, can be adjusted by varying the thicknesses of the two layers. The elastic and thermodynamic model developed in this paper is applicable to many other multilayer systems.

Acknowledgements

This project was supported by Grants PolyU 5322/04E, GYF66, GYF53. Co-author B.W. is also grateful for support from the National Science Foundation of China (Nos. 50232030, 10172030, 10572155 and 10732100) and the Science Foundation of Guangzhou Province (2005A10602002).

References

[1] Smith RC. Smart material system: model development. SIAM, Society for Industrial and Applied Mathematics; 2005.
[2] Ball BL, Smith RC, Ounaies Z. Smart Struct Mater 2003;5049:100.
[3] Chopra H, Ji C, Kokorin V. Phys Rev B 2000;61:4913.
[4] Chen X, Fang DN, Hwang KC. Acta Mater 1997;45:3181.
[5] Dapino MJ, Smith RC, Flatau AB. IEEE Trans Magn 2000;36:545.
[6] Li G, Furman E, Haertling GH. J Am Ceram Soc 1997;80:1382.
[7] Li X, Shih WY, Aksay IA, Shih WH. J Am Ceram Soc 1999;82:1733.
[8] Ludwig A, Quandt E. J Appl Phys 2000;87:4691.
[9] Nasser SN. J Appl Phys 2002;92:2899.
[10] O'Handley RC, Murray SJ, Marioni M, Nembach H, Allen SM. J Appl Phys 2000;87:4712.
[11] Uchino K. Piezoelectric actuators and ultrasonic motors. Boston (MA): Kluwer Academic Publishers; 1997.
[12] Lam KH, Sun CL, Chan HLW, Zhao XZ, Choy CL. J Electroceram 2007;18:251.
[13] Kugel VD, Chandran S, Cross LE. Appl Phys Lett 1996;69:2021.
[14] Newnham RE, Dogan A, Xu QC, Onitsuka K, Tressler J, Yoshikawa S. Proc IEEE Ultra Symp 1993;1:509.
[15] Fernandez JF, Dogan A, Fielding JT, Uchino K, Newnham RE. Sensor Actuat A Phys 1998;65:228.
[16] Wise SA. Sensor Actuat A 1998;69:33.
[17] Yoon CB, Lee SH, Lee SM, Kim HE. J Euro Ceram Soc 2006;26:2345.
[18] Zhang XC, Xu BS, Wang HD, Wu YX. Thin Solid Films 2005;488:274.
[19] Mossi K, Mouhli M, Smith BF, Mane PP, Bryant RG. Smart Mater Struct 2006;15:1785.
[20] Pertsev NA, Zembilgotov AG, Tagantsev AK. Phys Rev Lett 1998;80:1988.
[21] Bhattacharya K, James RD. J Mech Phys Solids 1999;47:531.
[22] Wang B, Woo CH. Acta Mater 2004;52:5639.
[23] Wang B, Woo CH. J Appl Phys 2005;97:084109.
[24] Wang B, Woo CH. J Appl Phys 2006;100:044114.
[25] Van Vleck JH. The theory of electric and magnetic susceptibility. Oxford University Press; 1932. p. 27–9.
[26] Wang J, Zhang TY. Acta Mater 2007;55:2465.
[27] Zheng Y, Wang B, Woo CH. Appl Phys Lett 2006;88:092903.
[28] Kim DJ, Jo JY, Kim YS, Chang YJ, Lee JS, Yoon JG, et al. Phys Rev Lett 2005;95:237602.

[29] Metha RR, Silverman BD, Jacobs JT. J Appl Phys 1973;44:3379.
[30] Lines ME, Glass AM. Principles and applications of ferroelectrics and related materials. Oxford: Clarendon Press; 1977.
[31] Hsueh CH. J Cryst Growth 2003;258:302.
[32] Hsueh CH, Evans AG. J Am Ceram Soc 1985;68:241.
[33] Hsueh CH, Lee S, Chuang TJ. J Appl Mech 2003;70:151.
[34] Freund LB, Nix WD. Appl Phys Lett 1996;69:173.
[35] Roytburd AL, Slutsker J. Appl Phys Lett 2006;89:042907.
[36] Zheng Y, Wang B, Woo CH. Appl Phys Lett 2006;89:083115.
[37] Zheng Y, Woo CH, Wang B, Zhu ZY. Appl Phys Lett 2007;90:092905.
[38] Zheng Y, Wang B, Woo CH. Appl Phys Lett 2006;89:062904.
[39] Zheng Y, Wang B, Woo CH. J Mech Phys Solids 2007;66:1661.
[40] Kwak BS, Erbil A, Budai JD, Chrisholm MF, Boatner LA. Phys Rev B 1994;49:14865.
[41] Li S, Eastman JA, Vetrone JM, Foster CH, Newnham RE, Cross LE. Jpn J Appl Phys 1997;36:5169.